Title

Limits on the morphogenetic role of rain splash transport in hillslope evolution

Journal

Journal of Geophysical Research Earth Surface, 121(3)

ISSN

2169-9003

Authors

Dunne, Thomas
Malmon, Daniel V
Dunne, Kieran BJ

Publication Date

2016-03-01

DOI

10.1002/2015jf003737

Peer reviewed

AGU PUBLICATIONS

JGR

Journal of Geophysical Research: Earth Surface

RESEARCH ARTICLE
10.1002/2015JF003737

Key Points:
- There is a dearth of mechanistic sediment transport equations for hillslope evolution modeling
- A rain splash equation driven by climatic effects scales up to morphogenetic timescales
- The resulting model was used to analyze constraints on the evolution of convex hillslope profiles

Correspondence to:
T. Dunne,
tdunne@bren.ucsb.edu

Citation:
Dunne, T., D. V. Malmon, and K. B. J. Dunne (2016), Limits on the morphogenetic role of rain splash transport in hillslope evolution, *J. Geophys. Res. Earth Surf.*, *121*, doi:10.1002/2015JF003737.

Received 23 SEP 2015
Accepted 16 FEB 2016
Accepted article online 18 FEB 2016

Limits on the morphogenetic role of rain splash transport in hillslope evolution

Thomas Dunne[1], Daniel V. Malmon[2], and Kieran B. J. Dunne[3]

[1]Bren School of Environmental Science and Management and Department of Earth Science, University of California, Santa Barbara, California, USA, [2]CH2M, Portland, Oregon, USA, [3]Department of Earth and Environmental Science, University of Pennsylvania, Philadelphia, Pennsylvania, USA

Abstract An experimentally parameterized equation for rain splash transport was generalized in order to compute annual sediment transport rates for a range of climates. The resulting equation was then used to examine the conditions under which rain splash transport can play a significant morphogenetic role in water-eroded landscapes. Rain splash can generate convex hillslopes on short, steep hillslopes such as the margins of gullies in unconsolidated sediments. However, comparison of predicted profiles with long, convex hillslopes in postorogenic landscapes indicates that rain splash cannot transport sufficient quantities of sediment to produce the observed convex hillslope profiles. Rates of biogenic transport estimated from the literature also appear to be insufficient. Sheetwash transport appears to be the only process capable of molding these extensive convex hillslope profiles despite the common assumption that it generates exclusively concave forms.

1. The Role of Rain Splash in Hillslope Evolution

Gilbert's [1877] concept of landforms evolving as the result of local imbalances between the supply and removal of regolith became an operational tool in geomorphology through the process-based algebraic analyses by *De Ploey and Savat* [1968] and the more exact analytic formulations by *Culling* [1960], *Kirkby* [1971], and *Hirano* [1975]. This paradigm is now expressed for one-dimensional hillslope evolution under transport-limited conditions as

$$\frac{\partial z}{\partial t} = -\frac{\partial Q_s}{\partial x} \tag{1}$$

where $\partial z/\partial t$ is the local rate of elevation change, x is horizontal distance, and Q_s is the volumetric transport rate of soil per unit width of hillslope ($m^3\,m^{-1}\,a^{-1}$). Equation (1) was developed into a quantitative tool for analyzing the relationship between hillslope form and sediment transporting processes [*Kirkby*, 1971; *Ahnert*, 1976], time [*Hirano*, 1968, 1975], and boundary conditions [*Hirano*, 1969; *Armstrong*, 1987]. The paradigm has been applied to various field problems, such as the dating of fault and wave-cut scarps [*Nash*, 1980; *Hanks et al*., 1984], terrace scarps [*Pierce and Colman*, 1986], and glacial moraines [*Bursik*, 1991], and incorporated into numerical simulations of landscape evolution [*Ahnert*, 1976; *Kirkby*, 1989; *Willgoose et al*., 1991]. Much of the work using (1) has assumed possible forms of sediment transport equations for Q_s to derive the generalized hillslope profiles such equations produce when subject to chosen boundary conditions [*Hirano*, 1969, 1975; *Kirkby*, 1971]. In particular, it was illustrated that processes characterized by sediment transport equations of the form

$$|Q_s| = K\left|\frac{dz}{dx}\right|^b \tag{2}$$

predict the evolution of convex profiles under the conditions where sediment is absorbed by the lower boundary at a decreasing or constant elevation. In the most common applications of this equation b is assumed to be 1.0, leading to the combination of (1) and (2) into the diffusion equation [*Culling*, 1960] with K defined as a morphological diffusivity ($m^3\,m^{-1}\,a^{-1}$) in the sense clarified by *Roering et al*. [2002]. If $b \neq 1.0$, the coefficient of (2) becomes more complex to define and is not simply a scalar diffusivity, as it depends on the relationship between local gradient and an effective coefficient of friction or critical slope angle for rapid transport [*Roering et al*., 2001] or a relationship between gradient and biotic activity [*Gabet et al*., 2003]. The evolution of hillslope profiles and associated sediment transport under such circumstances have been illustrated by, for example, *Ahnert* [1976], *Fernandes and Dietrich* [1997], and *Roering et al*. [1999].

In using (2) we are aware that there is a certain amount of confusion in the geomorphological literature about the use of the term "diffusion." Transport processes such as rain splash and various forms of bioturbation are traditionally referred to as "diffusive" when they actually create an advective sediment flux which is affected by gradient but not by downslope water flux in the manner of sheetwash. The effect of the water flux dependency in the latter case results in significantly greater average particle speeds or travel distances. However, the characterization of rain splash and bioturbation as diffusive has become refractory in geomorphology, because of the utility of the diffusion equation for providing solutions to (1) when transport actually does vary only with gradient and because the processes tend to smooth out undulations in topography. Thus, recent treatments of these smoothing processes [e.g., *Perron et al*., 2009; *Sweeney et al*., 2015] refer to rain splash as diffusive, and in the rest of the paper, we will follow the lead of these authors and refer to K as a diffusivity in the sense of a morphological diffusivity and only where transport varies linearly with gradient.

The upper convex portions of hillslope profiles in soil-mantled landscapes have traditionally been interpreted as fundamentally different in origin from planar or concave hillslopes and have elicited different suggestions concerning their formation. In humid landscapes, where various kinds of soil creep, often driven by bioturbation processes, dominate the transport of soil, this process has been interpreted as forming the upper convexity [*Gilbert*, 1909; *Kirkby*, 1971; *Roering et al*., 1999]. A few field-based estimates of K in (2) have recently become available for such areas, based on analyses of profile form, colluvium accumulation rates, and cosmogenic isotope loading (see summary by *Fernandes and Dietrich* [1997]), and the value of b has been evaluated in fewer cases where the sediment transport process or processes have been identified in a general way [*McKean et al*., 1993; *Roering et al*., 2001]. Attempts to isolate and quantify largely biogenic sediment transport processes in humid regions have resulted in transport equations that are not linear with gradient [*Gabet et al*., 2003].

In subhumid landscapes, with sparse vegetation cover and little evidence for intense bioturbation (e.g., termite mounds, soil macrofauna, or soil overturning by larger animals [*Paton et al*., 1995]), the upper convexity has usually been interpreted as the result of rain splash [*Kirkby*, 1971; *Mosley*, 1973]. Estimates of K and b for rain splash are even rarer than those for creep in humid environments. *Poesen and Savat* [1981] used laboratory experiments on reconstituted soils to develop an expression for rain splash transport as a function of rainfall kinetic energy, soil detachability, and local gradient. The equation predicts transport to be an approximate power function of gradient with $b \approx 0.75$, and although the equation does not isolate a simple K value, it can be used to compute hillslope erosion with (1). *Poesen* [1986] used the same equation to compute K values of $3.3–17 \times 10^{-4}\,m^2\,a^{-1}$ for bare soils, depending on their texture, though the method was not specified. Thus, although there is general agreement that rain splash obeys a sediment transport equation of the general form of (2) and that it would thus tend to generate convex hillslope profiles, little attention has been given to the absolute intensity of rain splash as represented by the constant, K, and whether this process can actually generate profiles with the length and degree of convexity observed in actual water-eroded landscapes over realistic timescales.

Most references to convex hillslopes in water-eroded landscapes relate to hilltops in badlands [e.g., *Mosley*, 1973; *Sweeney et al*., 2015] which range in length from meters to tens of meters and have gradients of 0.5 or more. However, in postorogenic landscapes in cratonic lowlands such as large areas of Africa, South America, and the central United States, many water-eroded hillslopes have gradients of only a few percent and convexities >100 m long. This paper refers particularly to these long, low-gradient convex hillslopes. *Chadwick et al*. [2013] provide a description of one such landscape. The paper also presents a general approach to upscaling transport equations from experimental studies of identifiable processes to predict long-term evolution of landforms.

2. Aims of the Paper

The purpose of this paper is to combine a rain splash transport equation parameterized from field and laboratory experiments [*Dunne et al*., 2010] with frequency distributions of rainstorm intensity and duration to develop a method of predicting annual transport rates, similar to (2), under a range of environmental conditions, particularly related to climate and its associated vegetation cover in grasslands. We also examine the limits of this transport process for shaping hillslope convexities where it is claimed to be the dominant morphogenetic agent over landforming timescales.

3. Computation of Rain Splash Transport for a Storm

Furbish et al. [2007] examined the fluid mechanical basis of rain splash transport in the absence of runoff through an analysis of single-drop rain splash experiments on sands. Small raindrops infiltrated the highly permeable surface without splashing, but larger drops decelerated sufficiently slowly upon impact to spread laterally, pushing up a small dilated perimeter ridge of grains which expanded outward with intense grain-to-grain collisions before some grains were launched on low-angle trajectories. There was a distribution of launch speeds and angles with a concentration toward lower values of each. Drops falling onto inclined sand surfaces created asymmetrical patterns of flow spreading, momentum transfer, and the distance and number of particles mobilized. Measurements of the resulting exponential distributions of splash distances for samples of single-drop impacts on horizontal surfaces were used together with the calculation of slope-directed momentum distribution to calculate downslope sand transport per unit of rainfall depth. The results predicted an essentially linear relationship between transport and hillslope gradient.

Dunne et al. [2010] developed a rain splash transport equation for single rainstorms in the absence of runoff, based on single-drop laboratory measurements of splash and experiments on a field soil under artificial rainfall. They collated laboratory results to quantify the slope-modulated momentum partitioning of the initial particle excitation and a range of launch angles and speeds of ballistic trajectories to compute transport distances. Ballistic transport outside of the dense grain collision zone observed by *Furbish et al*. [2007] appeared to be greater in the field experiments on natural soils than the trajectories described for the laboratory experiments on sand because the measured permeability of the natural surface was only ~5–33% of those in the Furbish experiments, leaving more of each drop to shear the sediment surface for a longer time. Also, although the median particle size of the sandy clay loam soil was similar to the finest sand studied by *Furbish et al*. [2007], 27% of the soil was finer than sand [*Dunne et al*., 2010, Figure 1].

Dunne et al. [2010] used the field experimental results to calibrate the effects of median drop size and ground cover density on mass mobilization per unit of rain. They also collated data from previous laboratory experiments to analyze the sensitivity of mobilization to a range of unaggregated soil textures. That compilation [*Dunne et al*., 2010, Figure 11] indicated that the selected sandy clay loam was close to the most easily mobilized textural class and that mobilization would decline sharply as particle size varied in either direction from this maximum. However, no attempt was made to calibrate the equation to a full range of soils including cohesive, aggregated, hydrophobic, or dispersive soils. The model predicted *Poesen*'s [1986] results for bare soils, and the *Furbish et al*. [2007] model behaved similarly over the range of gradient when its momentum partitioning function was calibrated to the field experiments.

The equation developed by *Dunne et al*. [2010] is

$$q = -aD^j e^{fC/D}\left[\frac{F\int_{\pi/2}^{3\pi/2}\Omega(\theta)\cos\theta\,\mathrm{d}\theta + (1-F)\int_{-\pi/2}^{\pi/2}\Omega(\theta)\cos\theta\,\mathrm{d}\theta}{\sqrt{2}\sqrt{1+\cos 2\alpha_0}}\right] \tag{3}$$

where

$$\Omega(\theta) = \frac{\left(2\cos\theta\sec\beta\sin\alpha_0\tan\beta + \sqrt{2}\sqrt{1+\cos(2\alpha_0)\sec^2\beta + \cos(2\theta)\tan^2\beta}\right)}{\left(\cos^2\theta\sec^2\beta + \sin^2\theta\right)\cos\beta} \tag{3a}$$

and q is the creep and aerial rain splash transport per unit depth of rainfall (kg m^{-1} mm^{-1}), D is the median raindrop size of the storm (mm), C is the ground cover density (decimal fraction), α_0 is the initial splash trajectory angle relative to the hillslope plane (sparse laboratory data suggest a dependence on particle size), β is the hillslope angle, and θ is the radial angle around the point of impact. The expression outside the bracket in (3) summarizes the effects of raindrop size, cover density, and soil detachability, a, on the magnitude of the initial splash. The model parameters, $a = 0.00104$, $j = 0.927$, and $f = -10.28$, were derived from field experiments on the sandy clay loam soil with a median grain size of 0.187 mm and bulk density of 1300–1600 kg m^{-3} in a grassland in Amboseli National Park, southern Kenya. The range of planimetric grass cover density used was 0.01–0.88; the range of grass height was 1–10 cm with occasional stems 20 cm high, and the simulated rainfall had a range of volumetric median drop sizes of 1.05–2.5 mm impacting at

approximately their terminal velocities. The value of a can be adjusted for other soil textures with the aid of Figure 11 in *Dunne et al.* [2010].

The integrals in the bracketed expression of (3) without the F terms represent the width-averaged downslope and upslope radial distances of splash relative to the horizontal. The expression varies almost linearly from 0 to 1.22 as $\tan\beta$ ranges from 0 to 1.0. The effects of downslope (F) and upslope ($1-F$) momentum partitioning were determined through compilation of laboratory results from other researchers. The value of F depends on local gradient over the full range of experimental observations up to approximately 45°:

$$F = 1 - 0.5\exp(-2.2\tan\beta), \tag{4a}$$

but for slopes of less than 25° the function was essentially linear:

$$F = 0.5 + 0.86\tan\beta. \tag{4b}$$

Combination of F with the integrals of (3) results in the net transport ranging from 0 to about 3.2 over $0 < \tan\beta < 1.0$ for the exponential case and over $0 < \tan\beta < 0.5$ for the linear case. Equation (3) must be multiplied by rainfall depth, p (mm), to compute the soil transport in a rainstorm:

$$q_{\text{storm}} = pq \tag{5}$$

where q_{storm} (kg m^{-1}) is the net downslope transport due to raindrop impacts in a storm of depth p (mm) in the absence of runoff.

Equation (3) includes the effects of three climatically determined factors. The influence of p on transport is linear for a single storm. The median drop size (D) is generally considered to relate to the intensity of each rainstorm [e.g., *Hudson*, 1971], although with considerable variability. Finally, the ground cover density (C) should in some way be related to the annual sum of the p values, comprising the total annual rainfall [e.g., *Nicholson et al.*, 1990, Figure 14a], although C might vary with season, soil type, and grazing pressure, especially in grasslands that are heavily stocked by managed herds. The effectiveness of ground cover density in reducing rain splash depends on the median drop size (3), being far more effective in reducing splash for small raindrops than for larger ones. The exponential decline of transport with increasing cover is stronger than the commonly assumed linear effect of $(1-C)$, presumably because the planform vegetation cover reduces raindrop impact while the associated density of erect stems reduces lateral splash distances. Since p, D, and C are climatic effects, we relate them to a widely available climatic characteristic: mean annual rainfall, which might even be estimated eventually from paleoclimatic information.

4. Computation of Rain Splash Transport in a Climatic Regime

In order to compute the long-term rain splash transport over landforming timescales, it is necessary to sum storm total transport rates from (5) over the frequency distributions of all values of storm duration and rainfall intensity in the storms that constitute the rainfall climate of a region. The value of K in (2) is then the rate at which the annual transport rate increases linearly with gradient under the condition that $b = 1.0$; when $b \neq 1.0$, the nonlinear rate of increase of transport with gradient is still the fundamental determinant of the rate at which rain splash can shape hillslopes. Our strategy for incorporating (3) into (5) and then (2), therefore, involves (i) relating ground cover density to mean annual rainfall from regional field measurements and (ii) developing a global relationship between median raindrop size and rainstorm intensity. With these values, it is possible to calculate transport per rainstorm for any hillslope gradient with (5). We then develop relationships between mean annual rainfall and the frequency distributions of rainstorm intensity (I) and duration (T) in order to obtain all values of I and p ($= IT$) that constitute the rainfall climate of a region. Finally, the rain splash transport per unit of hillslope width for any hillslope gradient is summed over all the values of p comprising the annual rainfall climate.

4.1. Relationship Between Climate and Ground Cover Density

Besides controlling the frequency of rainstorms of various intensities and durations, mean annual rainfall strongly affects the density of ground cover [*Nicholson et al.*, 1990]. Late-dry-season average ground cover

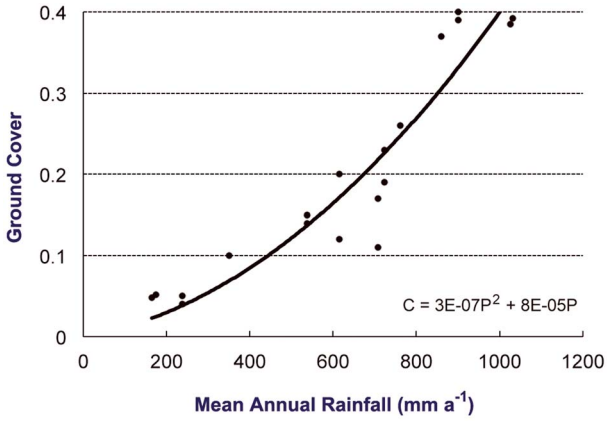

Figure 1. Basal ground cover at the end of a dry season for stations throughout the semiarid zone of Kenya, measured visually with a quadrat sampler.

density values were accumulated from the monthly monitoring records of the Kenya Rangeland Ecological Monitoring Unit of the Kenya Ministry of Tourism and Wildlife for various climatic regimes throughout Kenya. The estimates were made visually by field technicians with the aid of a 0.5 m square quadrat sampler [*Greig-Smith*, 1983]. We employed the same technique to measure ground cover on our experimental plots; standard errors among observers averaged 4.7% of the mean cover density for each plot.

In most parts of East Africa rainfall occurs in two 1 to 2 month long seasons, separated by longer dry periods. Since the rainy seasons are short and significant growth of ground cover lags the rain by about 1 month, most of the rain falls on the basal cover, i.e., that portion of the vegetative cover present at the end of each dry period. *Dunne et al*. [2011] illustrate an experimental case of this for the calibration site. *Nicholson et al*. [1990] measured a similar lag between the onset of rainfall and satellite measurements of vegetation cover across East Africa and the Sahel. *Schmidt and Karnieli* [2000, p. 56] also recorded that "[Annual plants] show a significant response only after a few weeks from the beginning of the rainy season" in the Negev Desert. We recognize, however, that the application of all rainfall energy to the basal cover must result in a maximum estimate of sediment mobilization by rain splash alone, especially in longer-than-average rainy seasons, but the computations could be refined with a graph of vegetation response time.

Figure 1 is a plot of the fractional cover density (C) at the beginning of both rainy seasons against mean annual rainfall (P, mm a^{-1}). The measured cover density did not differ significantly between the beginnings of the two rainy seasons, so a polynomial expression was fitted to the entire data set:

$$C = 3\times10^{-7}P^2 + 8\times10^{-5}P \tag{6}$$

$r^2 = 0.89$, $n = 28$, and $p < 0.001$.

4.2. Relationship Between Median Raindrop Size and Rainfall Intensity

Since rainfall records report only the frequency of storms of various intensities and durations rather than drop size, we first developed a relationship between median drop diameter and rainfall intensity using data from the literature. Numerous authors have investigated the relationship between raindrop size and rainfall intensity. *Laws and Parsons* [1943], citing their measurements from Washington, D.C., concluded that the volumetric median drop diameter varied by only 3 drop diameters over the range of natural rainfall intensities. *Hudson* [1963] in southern Africa and *Carter et al*. [1974] and *McGregor and Mutchler* [1976] in the southeastern United States noted that when measurements were extended to high intensities, there appeared to be an upper limit on raindrop size, beyond which drops break apart, and that a peak drop size occurred in the 60–100 mm h^{-1} range. Additional data from five other regions were added to the compilation, as indicated in the caption of Figure 2. Various claims have been made about regional differences in this relationship, which is characterized by considerable variability, but we are not aware of any robust regional differentiation. Therefore, the entire data set was fitted with a third-order polynomial, which predicts a maximum median drop diameter of 3.2 mm, 28% greater than the largest median drop size used to parameterize (3), at an intensity of 85 mm h^{-1} (Figure 2). The function

$$D = 1.22 + 5.46\times10^{-2}I - 4.53\times10^{-4}I^2 + 1.04\times10^{-6}I^3 \tag{7}$$

with $r^2 = 0.69$, $n = 242$, and $p < 0.0001$ was used to convert rainfall intensities into equivalent median drop sizes in the splash transport equation (3).

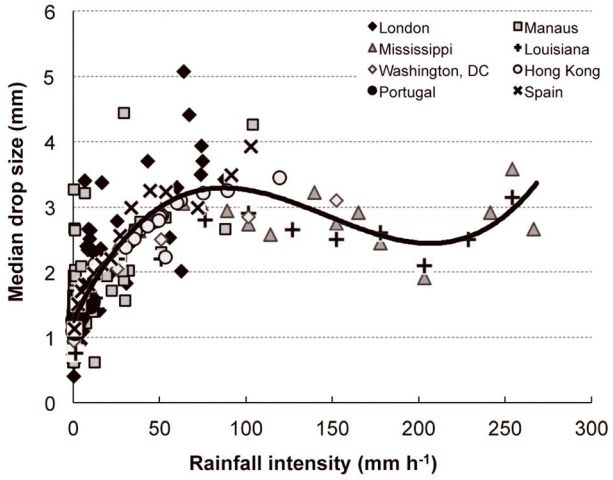

Figure 2. Global compilation of relations between median raindrop diameter and rainfall intensity. Data were compiled from London, UK [*Mason and Andrews*, 1960], Manaus, Brazil [*Brandt*, 1989], Mississippi, USA [*McGregor and Mutchler*, 1976], Louisiana, USA [*Carter et al*., 1974], Washington, DC, USA [*Laws and Parsons*, 1943], Hong Kong, PRC [*Jayawardena and Rezaur*, 2000], Portugal [*Coutinho and Tomás*, 1993], and southeast Spain [*Cerdà*, 1997]. Some data are obscured by overplotting.

4.3. Summation of Rain Splash Transport Over All Storms in a Climatic Regime

It is now possible to express the effects of C, D, and p in an annualized sediment transport equation in terms of the frequency distributions of rainstorm duration and intensity:

$$Q_s = \frac{1}{\rho_b} \sum_T \int_I \zeta(I,T) T q \mathrm{d}I \qquad (8)$$

where ρ_b is the soil bulk density (1450 kg m^{-3}), $\zeta(I, T)$ is the annual frequency (a^{-1}) of rainstorms of intensity I (mm h^{-1}), and duration T (h) and the drop size (D) values required to estimate q are provided by (7) for each intensity value in (8). East African rainfall records were employed to estimate $\zeta(I, T)$ because of their proximity to the original field area and because of the general uniformity of rainstorm-generating processes in the region. Mean annual rainfall at the 33 stations ranged from 225 to 2200 mm a^{-1} and included unimodal, bimodal, and trimodal seasonal regimes. More complex methods of accomplishing the same goal might be useful where the necessary rainfall records are available.

4.4. Rainfall Frequency Distributions for East Africa

Figure 3a shows the frequency distributions of rainfall intensity for storms of indicated durations (0.25–6 h) at a station 80 km northeast of the site at which the field experiments were conducted for calibration of (3). The distributions were developed from a tabulation of rainfall accumulations in various time periods, which although based on short weather records (9 years for this station) is the only such data source we are aware for the immediate region [*Lawes*, 1974]. To develop a more general expression for rain splash transport that could be applied more widely and in the absence of weather records, we correlated the parameters of the frequency distribution functions for rainstorm intensity and duration derived from these weather records with mean annual rainfall at 33 stations in Kenya, Tanzania, and Uganda. Record lengths ranged from 8 to 42 years at the time of the data publication, and there is a good chance that unpublished data from East Africa and elsewhere could provide a better test of the concept.

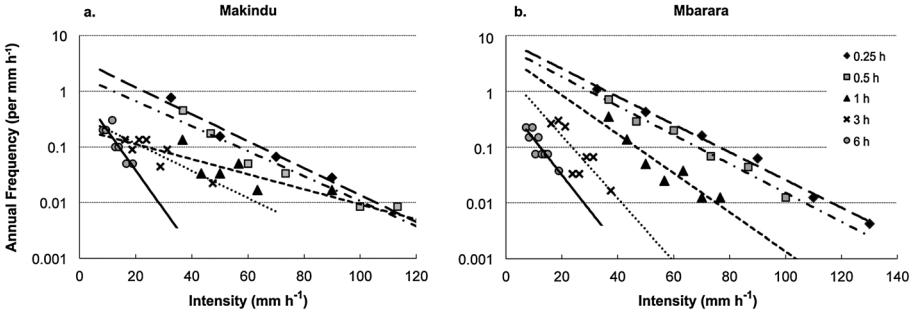

Figure 3. Frequency distributions of rainfall intensity for various storm durations at Makindu, Kenya (mean annual rainfall = 500 mm), and Mbarara, Uganda (mean annual rainfall = 880 mm).

The frequency distribution function of rainstorm intensity for each duration class, T, from 0.25 to 6 h was calculated for each station. Each function conforms to a two-parameter exponential distribution:

$$\frac{\zeta_{TI}}{\Delta I} = \chi e^{\lambda I} \tag{9}$$

where $\zeta_{TI}/\Delta I$ is annual frequency (events a^{-1}) of storms with intensity I (mm h^{-1}) occurring within an intensity bin ΔI, for each of the five modeled storm durations. There was no relationship between the slopes of the frequency distributions (λ) and mean annual rainfall for individual stations, but the standard deviations of these slopes were 17% of the mean for the 15, 30, and 60 min graphs and 30% for the 3 and 6 h graphs, which were based on fewer records. The slope parameter for a single storm duration depends solely on duration according to

$$\lambda = -0.043 - 0.032T \tag{10}$$

with $r^2 = 0.74$, $n = 153$, and $p < 0.001$.

Since the slopes of the distributions for each duration in Figure 3 remain relatively constant throughout the range of climate sampled by *Lawes* [1974], the regression constants (the intercepts at $I = 0$ in Figure 3) must increase with mean annual rainfall. This intercept was correlated with mean annual rainfall (P, mm) and the categories of storm duration (T, h) shown in Figure 3 as follows:

$$\chi = \frac{0.005P^{0.88}}{T^{0.55}} \tag{11}$$

for which $R^2 = 0.53$, $n = 153$, and $p < 0.001$.

The statistical model in (9)–(11) estimates values of χ and λ for distributions analogous to those shown in Figure 3 for any mean annual rainfall. The intensity ranges over which (10) and (11) were evaluated were determined by the East African data set [*Lawes*, 1974]. For 0.25, 0.5, and 1.0 h storms, only data from events exceeding intensities of 25 mm h^{-1} were reported. The lower limits for 3 h and 6 h storms were 15 mm h^{-1} and 5 mm h^{-1}, respectively. Thus, some portion of the lower intensity rainfall with smaller median raindrop sizes, below the critical size to create rain splash in sands [*Dunne et al.*, 2010, Figure 6], was not included in the analysis. Maximum recorded intensities were near 190 mm h^{-1}, 140 mm h^{-1}, 115 mm h^{-1}, 70 mm h^{-1}, and 35 mm h^{-1}, respectively for the five durations between 0.25 h and 6 h. The rain splash contribution of high-intensity storms near these limits was negligible over the long term since frequency in (9) decays exponentially with increasing intensity. For example, even where mean annual rainfall is 1500 mm, the total average annual contribution of rainfall from intensities above 125 mm h^{-1} is only 26 mm.

We assume that the statistical model developed for East African rainfall relates only to that climatic region and should not be extrapolated to cool, humid regions, for example. However, our method could be recalibrated or replaced in other regions. For example, *Hawk and Eagleson* [1992] mapped parameters for the Poisson rectangular pulse and the Bartlett-Lewis stochastic models of point rainfall over the United States on the basis of hourly rainfall totals from 74 weather stations.

4.5. Annual Rain Splash Transport Calculation

Since both cover density and the annual frequency distributions of rainfall duration and intensity (and therefore of drop size) were related to mean annual rainfall, we are in a position to evaluate the influence of climate on annual rates of rain splash transport for any hillslope gradient. First, the mean annual rainfall was used to estimate C by (6) and χ by (11). These χ values and the λ values from (10) were used to calculate a table of numbers of rainstorms in appropriate duration and intensity classes. Each value of I was assigned a drop size, according to (7). Equation (3) was then used to calculate q_{storm} for each cell in the (I,T) table for a range of hillslope gradient with p being calculated from the rainfall intensity and duration. The values of each q_{storm} were then multiplied by the number of storms for each (I,T) combination and summed using (8) to yield Q_s as a function of gradient and mean annual precipitation.

Equations (3) and (8) account for rain splash transport in the absence of a surface water film and thus are applicable to an entire landscape during the parts of rainstorms that do not exceed the soil's infiltration capacity. At the site of the field study, for example, final constant infiltration capacities of the sandy clay loam,

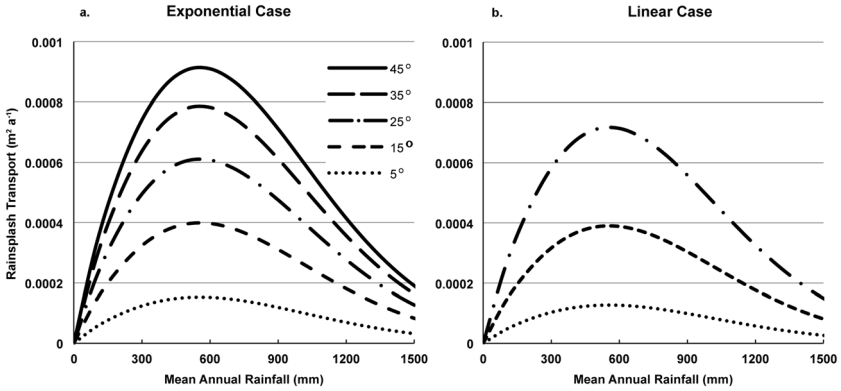

Figure 4. Relationship between annual rain splash transport and mean annual rainfall for a range of slope angles (β) as modeled by the cases in which (a) F behaves as in (4a) over a wide range of gradient and (b) F behaves as in (4b) for slope angles $<27°$.

measured with a sprinkling infiltrometer, range from about 10 to at least 80 mm h^{-1}, depending on rainfall intensity and local cover density [*Dunne et al.*, 1991, Figure 5]. Plot-averaged final infiltration rates are mainly in the range 22–35 mm h^{-1}, and transient rates during the first 10–30 min of storms are several tens of millimeters per hour higher [e.g., *Dunne and Dietrich*, 1980]. The transient portions of the infiltration curves last from 30 min for dry soils to 10 min for previously wet soils. Although the calibration sites are in a national park, they are grazed by cattle as well as by wild herbivores, which suggests that under entirely preanthropogenic conditions the infiltration capacities might have been even higher. The literature contains few reliable measurements (under sprinkling infiltrometers) in Africa or elsewhere to assess what infiltration capacities were before anthropogenic influences. If it is assumed, on the basis of our measured infiltration capacity curves, that storms up to 15–30 min long generate no significant surface water accumulation, then rainfall intensities for stations throughout East Africa (e.g., Figure 3) indicate that most of the rain falls without generating surface runoff. Of course, there is field evidence that sheetwash erosion does occur on these hillslopes during long rainstorms [*Dunne and Aubry*, 1985], but the limited extension of (3) into the few rainstorms that generate runoff provides a conservative upper bound on our calculated rain splash transport rates.

5. Results of Transport Calculations

Annual rain splash transport varies with mean annual rainfall (Figure 4), attaining a maximum at $P \approx 600$ mm, for a range of slope angles for both the nonlinear transport equation (using (4a)) and the linear approximation (using (4b)) over the restricted range of gradient $\tan\beta \leq 0.5$ (slope angles $<27°$). Figure 5 illustrates the

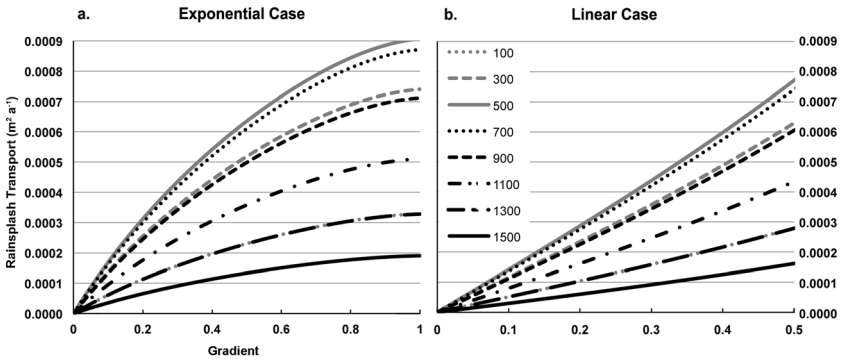

Figure 5. Relationship between annual rain splash transport and hillslope gradient for selected values of mean annual rainfall (mm a^{-1}) as modeled by the cases in which F is (a) an exponential function of $\tan\beta$ and (b) a linear function of $\tan\beta$. The curves for 100 mm a^{-1} and 1300 mm a^{-1} are essentially identical. Diffusivity values (m^2 a^{-1}) are the gradients of the lines in 5b.

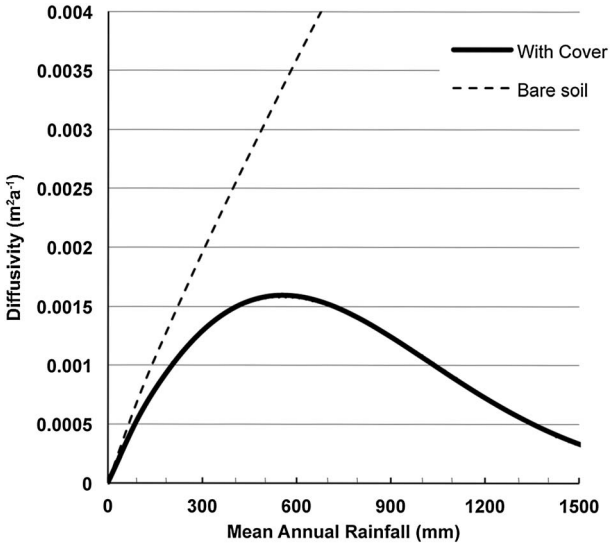

Figure 6. Relationship between morphological diffusivity and mean annual rainfall for vegetated soil (solid curve), obtained from the gradients of lines in Figure 5b, and for a bare soil (dashed curve) from the gradient of a calculation of annual transport for a bare soil under various annual rainfall amounts.

relationship between hillslope gradient and rain splash transport for selected mean annual rainfalls for each version of equations (4a) and (4b). The approximate linearity of Figure 5b allows us to estimate the morphological diffusivity in (2) from the slope of the line for each climate; its variation with mean annual rainfall is documented by the empirical relationship in Figure 6 for convenience, though the mathematical form of the functional relationship has no physical significance.

6. Discussion of Transport and Diffusivity Calculations

Comparison of Figures 4a and 4b or 5a and 5b indicates the effects of the raindrop momentum partitioning on F in (3) over two ranges of gradient. Experimental values of F compiled by *Dunne et al*. [2010] suggest that the downslope-oriented fraction of the detached soil increases with gradient at a slower rate as the gradient increases. Over a range of $\tan\beta \leq 0.5$, which would represent conditions where a fine-grained soil weathering from bedrock can be stabilized by grassy or shrubby vegetation in subhumid climates, the difference between the two functions is insignificant and the linear approximation used by *Furbish et al*. [2007] and *Dunne et al*. [2010] would be accurate. The nonlinear function might be useful for steep hillslopes eroding into thick, fine-grained sedimentary formations [*Mosley*, 1973; *Nash*, 1980; *Hanks et al*., 1984], steep, disturbed hillslopes [*Ghahramani et al*., 2012], tephra-covered volcano slopes [*Shimokawa and Taniguchi*, 1983; *Collins and Dunne*, 1986], or laboratory experiments [*Sweeney et al*., 2015] where it could make a difference up to approximately twofold in predictions. In the rest of our discussion of the morphogenetic role of rain splash transport we will analyze low-gradient hillslopes and therefore will adopt the linear approximation for the convenience of using the diffusivity metric, derived for that specific transport process.

Figure 4 indicates that for a given gradient, the climatic regime, through its offsetting influences on ground cover and the rainstorm intensity-duration regime, limits the diffusivity values for a particular soil type to a relatively narrow range. Figure 6 shows, for example, that for bare ground the diffusivity would be $63 \times 10^{-4}\,m^2\,a^{-1}$ under the rainfall energy of a $1500\,mm\,a^{-1}$ climatic regime, whereas the diffusivity predicted in the presence of vegetation for that rainfall is only $3 \times 10^{-4}\,m^2\,a^{-1}$. On the other hand, the diffusivity in a $100\,mm\,a^{-1}$ climate (with a basal cover of ~1%) is predicted to be $6 \times 10^{-4}\,m^2\,a^{-1}$, and diffusivity reaches a maximum of $16 \times 10^{-4}\,m^2\,a^{-1}$ at $P = 550\,mm$ (Figure 6). Increasing cover density diminishes splash transport at an exponential rate (3) because of its effects on both the area of soil exposed to drop impact and the filtering effects of plant stems on the resulting trajectories [*Dunne et al*., 2010]. In contrast, under the scenario of natural or artificial disturbance (fire, ashfall, and clearing) removing the ground cover the diffusivity increases monotonically with annual rainfall (Figure 6).

The nearly linear relationship between rain splash transport and mean annual rainfall for bare soil (Figure 6) is initially surprising since wetter climates have more intense rainstorms and thus larger drop sizes would be expected to cause more transport per unit of rainfall. However, the global relationship in Figure 2 predicts a maximum median drop size at an intensity of $85\,mm\,h^{-1}$ but little variation over the range 50–$200\,mm\,h^{-1}$. The rising drop size at intensities greater than $200\,mm\,h^{-1}$ has little effect on the total transport because of the low frequency of those intensities, even in wet climates.

There are few published estimates of morphological diffusivity for hillslopes in subhumid regions where water erosion processes are expected to dominate over biogenic and other forms of soil creep. The values

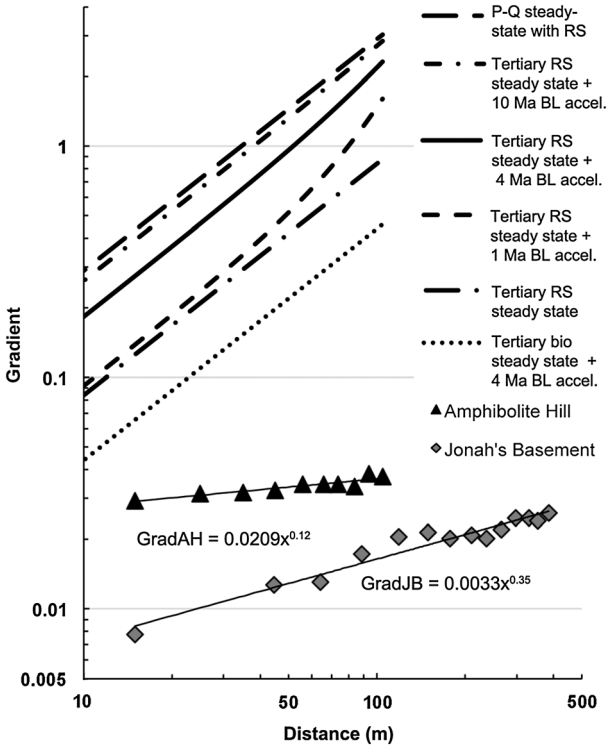

Figure 7. Symbols indicate the gradient profiles of the hillslopes Amphibolite Hill (AH) and Jonah's Basement (JB) on which the rain splash experiments were conducted at Eremito Ridge, Amboseli National Park, southern Kenya. The profiles were surveyed with tape and hand level. Gradient profiles are more revealing than elevation profiles for such long, gentle hillslopes. The five lines represent profiles computed for a 105 m long hillslope with equations (1) and (2) for various boundary conditions elaborated in the text.

listed by *Fernandes and Dietrich* [1997] for subhumid regions were back-calculated from steep fault scarp and terrace profiles with the assumption of linearity in equation (2) and uncertain initial conditions. The sediment transport process driving profile evolution was not identified but, according to the environmental conditions described, seems unlikely to be rain splash. By contrast, the values in Figure 6 are derived from experiments on rain splash alone and cover a range of up to $16 \times 10^{-4}\,m^2\,a^{-1}$ where mean annual rainfall is 500–600 mm a^{-1}. They are derived for a single soil type (sandy clay loam), and the variation with climate reflects the duration-intensity structure of the rainfall regime, the resulting median raindrop size for individual storms, and the effect of precipitation on ground cover density. The diffusivity values for most other soil types would be smaller than these values [*Dunne et al*., 2010, Figure 11].

7. Role of Rain Splash Transport in Hillslope Evolution

The convenience of the assumption that rain splash transport is a gradient-driven process not scaled by water flux led early analysts of hillslope profiles to conclude that rain splash was the process shaping the upper convexities of water-eroded hillslopes in subhumid regions [*Kirkby*, 1971; *Ahnert*, 1976]. *Dunne and Aubry* [1985] demonstrated with a field experiment that rain splash is sufficiently intense over short distances to stabilize the surface against incision by sheetwash. However, apart from the form of the proposed transport equation fitting efficiently into the diffusion equation with its prediction of smooth convex profiles, the issue was never raised of whether the intensity of rain splash could ever be responsible for the long, convex, and unchanneled portions of hillslopes in many water-eroded landscapes. A numerical solution of (1) with our rain splash equation supports the conclusion that for some very short, steep, and bare hillslopes such as the 1 m to several meters long convexities in the Wyoming badlands studied by *Mosley* [1973], rain splash transports sufficient quantities of sediment to shape initially steep planar gully margins into convexities within decades to centuries. However, in many other water-eroded postorogenic landscapes in subhumid regions hillslopes have unchanneled convexities up to hundreds of meters long connecting to even longer concave profiles. An obvious question arising from such an observation is whether rain splash transport, even if it obeys a transport equation of the appropriate mathematical form to produce convex profiles, is sufficiently intense to generate the observed convex profiles, given the constraints of time, climate, and boundary conditions.

Figure 7 shows the gradient-distance relationships of the hillslopes on which the rain splash field experiments were conducted in Amboseli National Park, Southern Kenya (2°33'S, 37°16'E). Gradients increase as power functions of distance to a maximum of 0.025 at 105 m on Amphibolite Hill and 0.037 at 387 m on Jonah's Basement although for the former case a linear function with a slope of $8 \times 10^{-5}\,m^{-1}$ also fits the measurements. The two hillslope profiles continue with concave portions that are approximately 600 m and 450 m long, respectively. The hillslopes are developed on Precambrian high-grade metamorphic rocks weathered to a sandy clay loam regolith 0.5–1 m deep.

Although there are no instrumental records of erosion and uplift rates for the region, long-term average lowering rates can be estimated from differences in the average elevations of erosion surface remnants deformed during the uplift associated with the Great African Rift Valley and mapped and dated by *Saggerson and Baker* [1965]. These remnants were compiled by *Dunne et al.* [1979, Figure 5] to estimate landscape lowering rates roughly for the Paleogene and Neogene periods and the late-Pliocene-Quaternary epochs. The resulting average land surface lowering rates in the vicinity of the rain splash experimental sites averaged 8.4 m Ma^{-1} for the first two periods (65–23 Ma and 23–4 Ma) and accelerated to 29 m $Ma^{-1}$for the last 4 Ma during gradual epeirogenic uplift, channel incision, and isostatic compensation. We are ignoring the regolith production mechanism and assuming that the general uniformity of soil depths close to 1 m in the region reflects that colluvium production has roughly kept pace with erosion throughout the fluctuations of climate and erosion. *Beauvais and Chardon* [2013] also used fragments of dated erosion surfaces across the cratonic landscapes of West Africa to estimate regionally averaged land surface erosion rates of 2–20 m Ma^{-1} (±10%) for roughly similar periods. *Chadwick et al.* [2013] measured erosion rates of 4 to 6 m Ma^{-1} on granites of the southeast African craton from ^{10}Be concentrations in the quartz fraction of river channel sediments.

If the convex profiles in Figure 7 are examined in the context of a steady state condition between uplift and erosion, E, the equilibrium profile, $z(x)$, obtained from the solution of (1) incorporating (2) with $b = 1.0$ is

$$z = \frac{E}{2K}\left[x_L^2 - x^2\right] \tag{12}$$

where x_L is the length of the convexity and $z = 0$ at $x = x_L$. The predicted gradient varies with distance according to

$$\frac{dz}{dx} = -\frac{E}{K}x. \tag{13}$$

In this calculation, it is assumed that the concave portions of the profiles on the lower few hundred meters of the hillslopes have also attained their own steady state form as the base level was lowered, so the inflection point at the end of the convexity is lowered at the same rate as the river at the base of the hillslope.

Inserting values of $E = 29 \times 10^{-6}$ m a^{-1} for the last 4 Ma into (12) along with $K = 10 \times 10^{-4}$ m^2 a^{-1} for rain splash transport (based on the local mean annual rainfall of 200 mm a^{-1} from Figure 6) predicts that the relief of the convexities in Figure 7 would be 160 m on Amphibolite Hill and 2172 m on Jonah's Basement whereas the surveyed values are 3.4 m and 7.9 m, respectively. The maximum gradients predicted by (13) would be 3.0 at $x_L = 105$ m on Amphibolite Hill and 11.0 at $x_L = 387$ m on Jonah's Basement. The entire steady state gradient profile for the convexity on Amphibolite Hill predicted from rain splash transport and the Pliocene-Quaternary lowering rate (uppermost line labeled P-Q in Figure 7) does not resemble the surveyed hillslopes. These values of relief and gradient, 1–2 orders of magnitude greater the measured values, would be required to remove the eroded sediment from the convexity in the extant climate if rain splash were the dominant process. Figure 7 also shows the steady state profile for rain splash transport with the Tertiary (65–4 Ma) base level lowering rate of 8.4×10^{-6} m a^{-1} and three numerically computed transient gradient profiles that would result if Amphibolite Hill had evolved from the Tertiary steady state profile and then responded to accelerated base level lowering of 29×10^{-6} m a^{-1} for 1 Ma, 4 Ma, and 10 Ma. The relaxation time for this hillslope (the time it would take the divide to erode at 1/e of the accelerated base level lowering after the perturbation) is approximately 4.5 Ma [*Mudd and Furbish*, 2007, equation (10)], and the signal propagation time (the time required for the erosion rate of the divide to respond to accelerated base level lowering) is 0.5 Ma, but the profile is predicted to converge on a new Pliocene-Quaternary steady state only after more than 10 Ma. None of the profiles considered are close to the measured ones, and no realistic rainfall diffusivity value from Figure 6 would bring the predicted profiles close to the field surveys.

Even if K were increased to 65×10^{-4} m^2 a^{-1}, obtained by calculating a diffusivity from the transport rates by burrowing animals on gradients <1.0 measured by *Gabet et al.* [2003, Figure 2], to allow for the possibility that there is transport by some yet unidentified bioturbation process on the Amboseli hillslopes, the predicted relief and gradients would still be unrealistically high (Figure 7). Again, this latter profile was calculated numerically after equilibration of base level lowering and bioturbation throughout the Tertiary followed by 4

million years of bioturbation with accelerated base level lowering. Diffusivity values derived from the *Gabet et al*. [2003] data for other bioturbation processes are much lower than the value used in Figure 7 making it even more unlikely that bioturbation could produce the Amboseli convexities.

On the other hand, the diffusivity required to balance the erosion rate with the observed maximum gradient of each profile would have to be $830 \times 10^{-4}\,m^2\,a^{-1}$ for Amphibolite Hill and $4600 \times 10^{-4}\,m^2\,a^{-1}$ for Jonah's Basement. Such diffusivity values are outside the range of our measured and modeled values for rain splash and outside the range of *K* values of $50–120 \times 10^{-4}\,m^2\,a^{-1}$, back computed from hillslope profiles and compiled by *Fernandes and Dietrich* [1997]. They are also much higher than diffusivity values that we fitted to published models of transport by root disturbance ($\sim 1–5 \times 10^{-4}\,m^2\,a^{-1}$), tree throw ($33 \times 10^{-4}\,m^2\,a^{-1}$), and burrowing animals ($65 \times 10^{-4}\,m^2\,a^{-1}$) in humid climates [*Gabet et al*., 2003]. The conclusion seems inescapable that small-scale granular disturbance of the kinds that are usually thought of as producing convex hillslope profiles is insufficient to generate the widespread long convexities in the field area of southern Kenya.

The same logic was applied to the long (75, 225, and 710 m) hillslopes surveyed by *Chadwick et al*. [2013] in a similar postorogenic, cratonic environment of southeastern Africa at three sites with mean annual rainfall of 450 mm, 500 mm, and 730 mm where the long-term erosion rates, measured with cosmogenic isotopes, were 5.9, 6.6, and 4 m Ma^{-1}, respectively. Utilizing the diffusivity values for rain splash transport in each climate derived from our rain splash calculations (Figure 6), the maximum gradients that would be in equilibrium with such erosion rates at the ends of the convex profiles would have to be 0.34, 1.14, and 2.54, whereas the measured gradients are 0.035, 0.06, and 0.08, respectively. Back-calculating required diffusivity values from these measured maximum gradients at steady state yields values of $126 \times 10^{-4}\,m^2\,a^{-1}$, $248 \times 10^{-4}\,m^2\,a^{-1}$, and $355 \times 10^{-4}\,m^2\,a^{-1}$, respectively. These diffusivities are again outside the range that has been associated with any granular disturbance process—whether rain splash or biogenic transport—and therefore are not likely to represent the mechanism that is shaping these long, convex hillslopes in slowly eroding postorogenic subhumid landscapes. Even in the tectonically active landscape of the Gabilan Mesa in the California Coast Ranges, our rain splash transport equation for a sandy soil (Soil Survey of San Benito County, California) and a mean annual rainfall of 320 mm a^{-1} [*Perron et al*., 2009] coupled with a conservatively low base level lowering rate of 100 m Ma^{-1} over 400 ka [*Page et al*., 1998] does not generate a profile even approximating the convex profile of the 45 m long hillslope representing the landscape measured by *Sweeney et al*. [2015].

Another indication that the observed hillslopes were not produced by a linear diffusive process is that the gradient profiles for the surveyed slopes are, in general, not linear functions of distance from the divide. In the Amboseli cases, power functions fit the topographic data better than linear functions, although for the shorter and steeper Amphibolite Hill, a linear function performs adequately while still implying a diffusivity of $3420 \times 10^{-4}\,m^2\,a^{-1}$ (Figure 7). In the southeast African cases, *Chadwick et al*. [2013, Figure 3] showed that gradient increased in proportion to the logarithm of drainage area per unit contour width, interpreted here to be approximately the same as hillslope distance for the smooth hillslopes.

On the convex hillslopes of their study area *Chadwick et al*. [2013] observed field evidence for variable but unknown amounts of rain splash, intermittent slopewash, and termite bioturbation at the drier sites and burrowing and tree turnover at the wetter site. At the Kenya sites, rain splash and slopewash appear to be the only candidate processes because termitaria and fossorial animals are rare and trees are sparse; low trees and bushes are occasionally torn up by elephants but without any apparent downslope bias. The only remaining candidate for evacuating sediment on such low gradients is sheetwash transport, which is usually interpreted to generate concave hillslope profiles during steady state or transient landscape evolution because it scales nonlinearly with flow (and therefore with downslope distance) [*Kirkby*, 1971; *Smith and Bretherton*, 1971; *Ahnert*, 1976; *Smith*, 2010]. However, this commonly assumed mathematical form of sheetwash transport equations describes only the instantaneous transport behavior assuming an idealized situation of steady, gradually varied flow or time-averaged conditions that mimic this condition, and not the integrated transport and sediment redistribution generated by the frequency distributions of rainstorm duration and intensity that constitute a climatic rainfall regime.

Dunne [1991] proposed that long, convex hillslopes could be produced by sheetwash erosion if the hillslopes had sufficient length, hydraulic roughness, and low gradient that their runoff concentration times (the time required for water to flow from the divide to the lower boundary) exceeded the duration of most rainstorms.

To support this proposal, an experimentally calibrated equation for sheetwash sediment transport as a function of flow rate, gradient, and ground cover density was combined with a nonsteady, nonuniform model of overland flow based on field-measured hydraulic properties to model the topographic evolution of an initially planar hillslope. The model was then forced with locally measured exponential frequency distributions of rainstorm intensities and durations to compute the evolution of the hillslope over thousands of years. The results demonstrated that if the climate generates a sufficient number of rainstorms that are shorter than the hillslope runoff concentration time, the upper part of the hillslope is eroded faster than the lower portion, tending to produce an upper convex profile in association with the efficiency of sheetwash transport. The degree and length of the convexity for a given initial hillslope length and gradient would thus reflect the moments of the rainstorm frequency distributions.

8. Conclusion

Combination of an experimentally calibrated rain splash transport equation with frequency distributions of rainstorm duration and intensity allows the calculation of long-term rain splash transport and the resulting hillslope evolution in a range of climates. Rain splash transport by itself is not sufficiently intense to generate observed long convex hillslope profiles in postorogenic environments with low drainage densities, although it can erode the short, steep convexities in badlands and along gully margins [*Mosley*, 1973]. Soil creep through bioturbation is also insufficient to generate observed long, low-gradient convexities, even if conservatively high empirical estimates of bioturbation from other regions are used to calculate the hillslope profiles. Quantification of transport processes emphasizes that the magnitude or intensity of a process, as driven by environmental controls such as climate and soil properties, limits the nature of landscape; the mathematical form of the transport equation alone is insufficient to define the necessary conditions for observed landforms.

The only transport process documented to be sufficiently intense to erode convexities of the appropriate scale in postorogenic environments with low drainage densities (long hillslopes) is sheetwash erosion, despite the common assumption in hillslope evolution theory that this process obeys a mathematical form that should produce concave hillslope profiles. This assumption was originally based on theory and experiments on localized, instantaneous sediment transport in rivers and on short plots. The integration of such expectations up to the scale of populations of weather events operating over the timescale of landform evolution and the spatial scale of long natural hillslopes results in convex hillslopes generated by sheetwash erosion under a widespread range of environmental conditions.

Acknowledgments
The work was supported by a grant from NSF Earth Science (EAR-8313172) with logistical support from the Kenya Rangeland Ecological Monitoring Unit. Data used in the analysis can be obtained from T. Dunne. The paper was improved by comments from David Furbish, Katerina Michaelides, and an anonymous reviewer.

References

Ahnert, F. (1976), Brief description of a comprehensive three-dimensional process-response model of landform development, *Z. Geomorphol. Suppl. Band*, *25*, 29–49.
Armstrong, A. C. (1987), Slopes, boundary conditions, and the development of convexo-concave forms—Some numerical experiments, *Earth Surf. Processes Landforms*, *12*, 17–30.
Beauvais, A., and D. Chardon (2013), Modes, tempo, and spatial variability of Cenozoic cratonic denudation: The West African example, *Geochem. Geophys. Geosyst.*, *14*, 1590–1608, doi:10.1002/ggge.20093.
Brandt, C. J. (1989), The size distribution of throughfall drops under vegetation canopies, *Catena*, *16*, 507–524.
Bursik, M. (1991), Relative dating of moraines based on landform degradation, Lee-Vining, California, *Quat. Res.*, *35*, 451–455.
Carter, C. E., J. D. Greer, H. J. Braud, and J. M. Floyd (1974), Raindrop characteristics in the south central United States, *Trans. Am. Soc. Agric. Eng.*, *17*, 1033–1037.
Cerdà, A. (1997), Rainfall drop size distribution in the Western Mediterranean basin, Valencia, Spain, *Catena*, *30*, 169–182.
Chadwick, O. A., J. J. Roering, A. M. Heimsath, S. R. Levick, G. P. Asner, and L. Khomo (2013), Shaping post-orogenic landscapes by climate and chemical weathering, *Geology*, *41*, 1171–1174.
Collins, B. D., and T. Dunne (1986), Erosion of tephra from the 1980 eruption of Mount St. Helens, *Geol. Soc. Am. Bull.*, *97*, 896–905.
Coutinho, M. A., and P. P. Tomás (1993), Characterization of raindrop size distributions at the Vale Formoso Experimental Erosion Center, *Catena*, *25*, 187–197.
Culling, W. E. H. (1960), Analytical theory of erosion, *J. Geol.*, *68*, 336–344.
De Ploey, J., and J. Savat (1968), Contribution à l'étude de l'érosion par le splash, *Z. Geomorphol.*, *12*, 174–193.
Dunne, T. (1991), Stochastic aspects of the relations between climate, hydrology and landform evolution, *Jpn. Geomorphol. Union Trans.*, *12*, 1–24.
Dunne, T., and B. F. Aubry (1985), Evaluation of Horton's theory of sheetwash and rill erosion on the basis of field experiments, in *Hillslope Processes*, edited by A. D. Abrahams, pp. 31–53, Allen and Unwin, London.
Dunne, T., and W. E. Dietrich (1980), Experimental study of Horton overland flow on tropical hillslopes. Part I: Soil conditions, infiltration, and frequency of runoff, *Z. Geomorphol. Suppl. Band*, *33*, 40–59.
Dunne, T., W. E. Dietrich, and M. J. Brunengo (1979), Rapid evaluation of soil erosion and soil lifespan in the grazing lands of Kenya, *Int. Assoc. Hydrol. Sci. Publ.*, *128*, 421–428.

Dunne, T., W. Zhang, and B. F. Aubry (1991), Effects of rainfall intensity, vegetation, and microtopography on infiltration and runoff, *Water Resour. Res.*, *27*, 2271–2285, doi:10.1029/91WR01585.
Dunne, T., D. V. Malmon, and S. M. Mudd (2010), A rain splash transport equation assimilating field and laboratory measurements, *J. Geophys. Res.*, *115*, F01001, doi:10.1029/2009JF001302.
Dunne, T., D. Western, and W. E. Dietrich (2011), Effects of cattle trampling on vegetation, infiltration, and erosion in a tropical rangeland, *J. Arid Environ.*, *75*, 58–69, doi:10.1016/j.jaridenv.2010.09.001.
Fernandes, N. F., and W. E. Dietrich (1997), Hillslope evolution by diffusive processes: The timescale for equilibrium adjustments, *Water Resour. Res.*, *33*, 1307–1318.
Furbish, D. J., K. K. Hammer, M. Schmeeckle, M. N. Borosund, and S. M. Mudd (2007), Rain splash of dry sand revealed by high-speed imaging and sticky paper splash targets, *J. Geophys. Res.*, *112*, F01001, doi:10.1029/2006JF000498.
Gabet, E. J., O. J. Reichman, and E. W. Seabloom (2003), The effects of bioturbation on soil processes and sediment transport, *Annu. Rev. Earth Planet. Sci.*, *31*, 249–273.
Ghahramani, A., I. Yoshiharu, and S. M. Mudd (2012), Field experiments constraining the probability distribution of particle travel distances during natural rainstorms on different slope gradients, *Earth Surf. Processes Landforms*, *37*, 473–485, doi:10.1002/esp.2253.
Gilbert, G. K. (1877), *Report on the Geology of the Henry Mountains, Utah*, U.S. Geogr. and Geol. Surv. of the Rocky Mt. Region, Washington, D. C.
Gilbert, G. K. (1909), The convexity of hilltops, *J. Geol.*, *17*, 344–350.
Greig-Smith, P. (1983), *Quantitative Plant Ecology*, 3rd ed., 359 pp., Univ. of Calif. Press, Berkeley.
Hanks, T. C., R. C. Bucknam, K. R. Lajoie, and R. E. Wallace (1984), Modification of wave-cut and faulting-controlled landforms, *J. Geophys. Res.*, *89*, 5771–5790.
Hawk, K. L., and P. S. Eagleson (1992), Climatology of station storm rainfall in the continental United States: Parameters of the Bartlett-Lewis and Poisson rectangular pulses models, *Rep*. *336*, 330 pp., Ralph M. Parsons Lab., Mass. Inst. of Technol., Boston.
Hirano, M. (1968), A mathematical model of slope development: An approach to analytical theory of erosional topography, *J. Geosci. Osaka City Univ.*, *11*, 13–52.
Hirano, M. (1969), Slope form and upheaval of the Yoro Mountain range, central Japan [in Japanese], *J. Geol. Soc. Jpn.*, *75*, 615–627.
Hirano, M. (1975), Simulation of developmental process of interfluvial slopes with reference to graded form, *J. Geol.*, *83*, 113–123.
Hudson, N. W. (1963), Raindrop size distribution in high intensity storms, *Rhod. J. Agric. Res.*, *1*, 6–11.
Hudson, N. W. (1971), *Soil Conservation*, 324 pp., Batsford Ltd., London.
Jayawardena, A. W., and R. B. Rezaur (2000), Drop size distribution and kinetic energy load of rainstorms in Hong Kong, *Hydrol. Processes*, *14*, 1069–1082.
Kirkby, M. J. (1971), Hillslope process-response models based on the continuity equation, *Inst. Br. Geogr. Spec. Publ.*, *3*, 15–30.
Kirkby, M. J. (1989), A model to estimate the impact of climatic change on hillslope and regolith form, *Catena*, *16*, 321–341, doi:10.1016/0341-8162(89)90018-0.
Lawes, E. F. (1974), *An Analysis of Short Duration Rainfall*, *Tech. Mem. 23*, 43 pp., East Afr. Meteorol. Dep., Nairobi.
Laws, J. O., and D. A. Parsons (1943), The relation of raindrop size to intensity, *Eos Trans. AGU*, *24*, 452–459.
Mason, B. J., and J. B. Andrews (1960), Drop-size distributions from various types of rain, *Q. J. R. Meteorol. Soc.*, *86*, 346–353.
McGregor, K. C., and C. K. Mutchler (1976), Status of the R factor in northern Mississippi, in *Soil Erosion: Prediction and Control*, pp. 135–142, Soil Conserv. Soc. of Am., Ankeny, Iowa.
McKean, J. A., W. E. Dietrich, R. C. Finkel, J. R. Southon, and M. W. Caffee (1993), Quantification of soil production and downslope creep rates from cosmogenic ^{10}Be accumulations on a hillslope profile, *Geology*, *21*, 343–346.
Mosley, M. P. (1973), Rainsplash and the convexity of badland divides, *Z. Geomorphol. Suppl. Band*, *58*, 81–91.
Mudd, S. M., and D. J. Furbish (2007), Responses of soil-mantled hillslopes to transient channel incision rates, *J. Geophys. Res.*, *112*, F03S18, doi:10.1029/2006JF000516.
Nash, D. B. (1980), Morphological dating of degraded normal fault scarps, *J. Geol.*, *88*, 353–360.
Nicholson, S. E., M. L. Davenport, and A. R. Malo (1990), A comparison of the vegetation response to rainfall in the Sahel and East Africa, using normalized difference vegetation index from NOAA AVHRR, *Clim. Change*, *17*, 209–241.
Page, B. M., G. A. Thompson, and R. G. Coleman (1998), Late Cenozoic tectonics of the central southern Coast Ranges of California, *Geol. Soc. Am. Bull.*, *110*, 846–876.
Paton, T. R., G. S. Humphreys, and P. B. Mitchell (1995), *Soils: A New Global View*, 213 pp., UCL Press, London.
Perron, J. T., J. W. Kirchner, and W. E. Dietrich (2009), Formation of evenly spaced ridges and valleys, *Nature*, *460*, 502–509, doi:10.1038/nature08174.
Pierce, K. L., and S. M. Colman (1986), Effect of height and orientation (microclimate) on geomorphic degradation rates and processes, late-glacial terrace scarps in central Idaho, *Geol. Soc. Am. Bull.*, *97*, 869–885.
Poesen, J. (1986), Field measurement of splash erosion to validate a splash transport model, *Z. Geomorphol. Suppl. Band*, *58*, 81–91.
Poesen, J., and J. Savat (1981), Detachment and transportation of loose sediments by raindrop splash. Part II—Detachability and transportability measurements, *Catena*, *8*, 19–41.
Roering, J. J., J. W. Kirchner, and W. E. Dietrich (1999), Evidence for nonlinear, diffusive sediment transport on hillslopes and implications for landscape morphology, *Water Resour. Res.*, *35*, 853–870.
Roering, J. J., J. W. Kirchner, L. S. Sklar, and W. E. Dietrich (2001), Hillslope evolution by nonlinear creep and landsliding: An experimental study, *Geology*, *29*, 143–146.
Roering, J. J., J. W. Kirchner, L. S. Sklar, and W. E. Dietrich (2002), Reply-Hillslope evolution by nonlinear creep and landsliding: An experimental study: Comment and reply, *Geology*, *30*, 482.
Saggerson, E. P., and B. H. Baker (1965), Post-Jurassic erosion surfaces in eastern Kenya and their deformation in relation to rift structures, *Q. J. Geol. Soc. London*, *121*, 51–72.
Schmidt, H., and A. Karnieli (2000), Remote sensing of the seasonal variability of vegetation in a semi-arid environment, *J. Arid Environ.*, *45*, 43–59.
Shimokawa, E., and Y. Taniguchi (1983), Debris yield from hillside slope of active volcano, in *Symposium on Erosion Control in Volcanic Areas, Seattle, July 1982*, pp. 155–181, Jpn. Public Works Res. Inst., Ibaraki, Japan.
Smith, T. R. (2010), A theory for the emergence of channelized drainage, *J. Geophys. Res.*, *115*, F02023, doi:10.1029/2008JF001114.
Smith, T. R., and F. Bretherton (1971), Stability and the conservation of mass in drainage-basin evolution, *Water Resour. Res.*, *8*, 1506–1529.
Sweeney, K. E., J. J. Roering, and C. Ellis (2015), Experimental evidence for hillslope control of landscape scale, *Science*, *349*, 51–53, doi:10.1126/science.aab0017.
Willgoose, G., R. L. Bras, and I. Rodriguez-Iturbe (1991), A coupled channel network growth and hillslope evolution model: 1. Theory, *Water Resour. Res.*, *27*, 1671–1684.